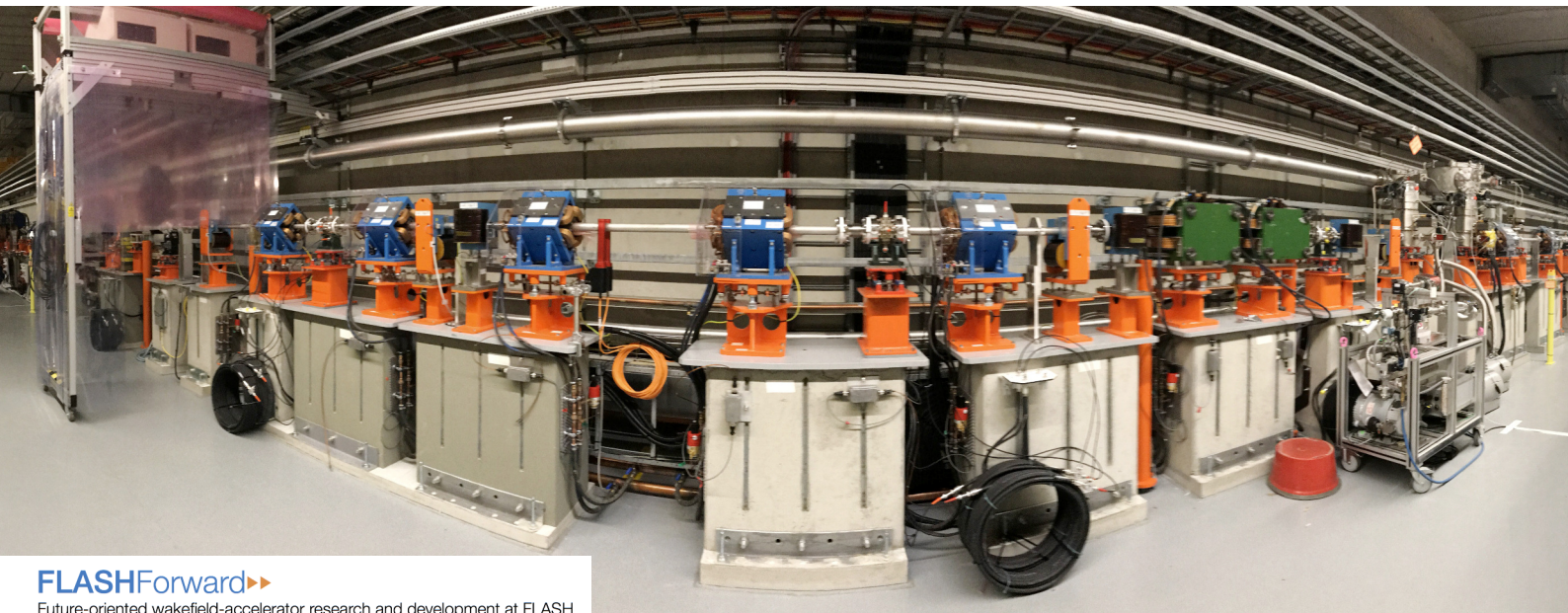




# Electron Spectrometer for FLASHForward Plasma-Wakefield Accelerator

Artemis Kontogoula  
Supervisor: Vladyslav Libov



**FLASHForward** ▶▶

Future-oriented wakefield-accelerator research and development at FLASH

September 7, 2017

National & Kapodistrian University of Athens, Greece  
Deutsches Elektronen-Synchrotron (DESY), Hamburg

# Contents

<b>1</b>	<b>Plasma-wakefield acceleration</b>	<b>3</b>
<b>2</b>	<b>FLASHForward experiment at DESY</b>	<b>4</b>
<b>3</b>	<b>Electron Spectrometer for FLASHForward</b>	<b>6</b>
<b>4</b>	<b>Magnetic field analysis</b>	<b>7</b>
4.1	DORIS III dipole magnet . . . . .	7
4.2	Magnetic Field Measurements . . . . .	7
4.3	One-dimensional field map . . . . .	8
4.4	Hysteresis Curve . . . . .	10
4.5	Three-dimensional field maps . . . . .	11
<b>5</b>	<b>Tracking simulations and resolution determination</b>	<b>12</b>
<b>6</b>	<b>Conclusions</b>	<b>14</b>
<b>A</b>	<b>Additional figures</b>	<b>15</b>

# 1 Plasma-wakefield acceleration

Charged particle accelerators are key instruments for science and technology. They play a central role in particle and nuclear physics, material science, molecular biology, medicine as well as in many other areas. However accelerators are very costly, require long design and construction times, and need a lot of resources for operation and maintenance. Moreover, for further advances in particle physics, even higher beam energies compared to what has been achieved up to now, are required, meaning even further increase of the size and cost of accelerators.

Plasma-wakefield acceleration [1, 2] (PWFA) is a new promising technique for accelerating charged particles which might lead to next-generation, compact accelerators for particle physics and other applications such as free-electron-lasers or medicine. The main idea is that plasmas support very strong electromagnetic fields, thus particles can be accelerated on very small distances, potentially leading to compact accelerators.

The principle of PWFA is illustrated in Figure 1. An intense electron bunch (so-called *drive bunch*) enters the plasma, an ionised gas consisting of ions and electrons. Due to a large electric field of the bunch, plasma electrons are expelled sideways, while ions practically don't move, since they are at least three orders of magnitude heavier than electrons. After the drive bunch has passed a certain distance, the expelled electrons are pulled back by the remaining ions, overshoot, and start an oscillating motion. As a result, an ion cavity, co-propagating with the drive beam, is formed, as shown on the Figure 1. Such charge separation leads to strong electromagnetic fields inside the ion cavity, called *wakefields* (e.g. electric fields can reach hundreds of GV/m). It is these fields which can be utilised to accelerate charged particles.

The described process is also called *beam-driven wakefield acceleration* (PWFA). Another possibility to excite the plasma-wakefields is to use an intense laser-pulse instead of a charged-particle beam, and is called *laser-driven wakefield acceleration* (LWFA).

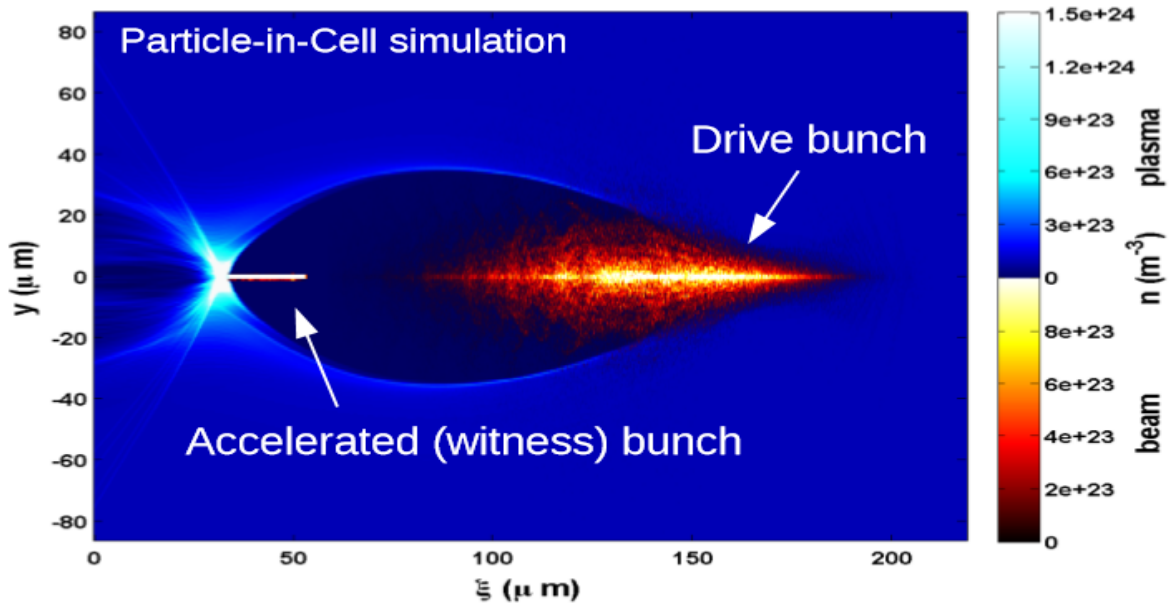


Figure 1: Plasma-wakefield acceleration principle. Plasma electron density is shown in blue, while drive bunch electron density is given in orange.

Beam-driven acceleration offers some advantages compared to the laser-driven, however is much less developed, due to scarce availability of accelerators.

## 2 FLASHForward experiment at DESY

FLASHForward [3] is a novel plasma-wakefield experiment at DESY (Hamburg, Germany), currently in the commissioning phase, aiming to fill the void in the area of beam-driven plasma-wakefield acceleration. It will use high-quality, GeV-class electron beams from the FLASH free-electron (FEL) laser to drive the wakefields. The scientific goals are threefold:

1. Generate high-quality electron beams with PWFA directly in the plasma (*internal injection*). The drive beam is injected into plasma, while the witness beam is created from the background plasma electrons. This is important because the resulting witness beams typically feature small emittance and durations, potentially interesting for applications such as FELs.
2. Demonstrate quality preservation of *externally-injected electron beams*. The method requires two bunches shot into plasma: the first one drives the wake (driver) and the second one is accelerated by the wake (witness). This technique is crucial for staging of plasma accelerators, a prerequisite for high-energy applications such as particle physics colliders.
3. Demonstrate FEL-gain using PWFA-accelerated beams. This would be a first proof-of-principle of plasma-powered FELs.

FLASH is an FEL user facility. In order to allow parasitic operation of FLASHForward, an independent beamline was constructed. The overall layout of the machine is shown in Figure 2. It consists of a superconducting linac, two undulator beamlines (FLASH1 and FLASH2) and the third, dedicated beamline for FLASHForward experiments.

The linac starts with a laser-driven radio-frequency (RF) gun, where the electron bunches are generated and accelerated to 5 MeV. The charge is variable from few tens of pC up to a few nC, and the bunch length is several ps. The subsequent superconducting RF modules accelerate electrons up to 1.2 GeV. The longitudinal charge density (current)

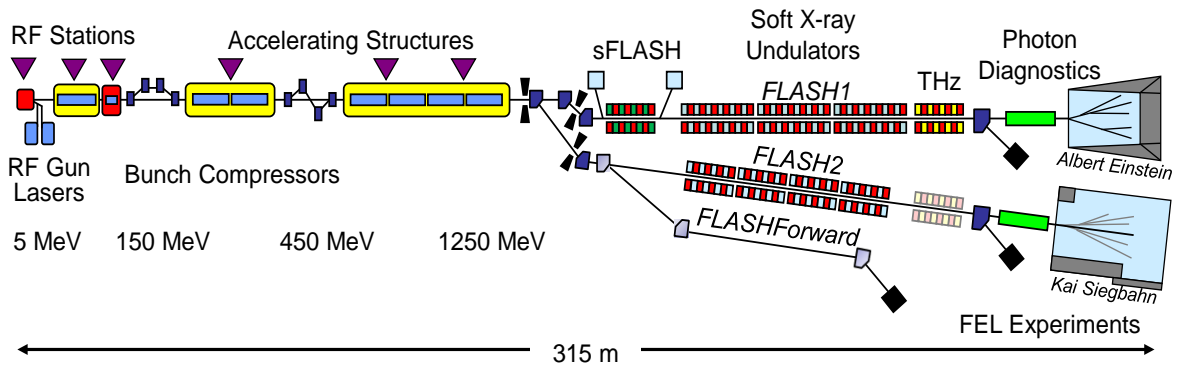


Figure 2: Layout of the FLASH facility, including the new FLASHForward plasma-wakefield acceleration beamline.

of the electron bunch is increased in the magnetic bunch compressors. After the linac, the beam is distributed between two undulator beamlines, FLASH1 and FLASH2, where photon radiation is produced.

FLASH1 undulator beamline consists of six 4.5 m long undulators with planar permanent magnet devices having a fixed gap of 12 mm and a magnetic field amplitude of 486 mT. Behind this section, the electron beam is separated from the photon beam by a strong vertically deflecting dipole, while the FEL radiation propagates to the experimental hall. FLASH2 has newer undulators with the possibility to change the gap between the magnetic poles of the undulator magnets; this changes the magnetic field and thus the wavelength of the radiation. With a beam energy given by the required wavelength of FLASH1, the experiment at FLASH2 is able to change the wavelength in a wide range for their experiment without influencing FLASH1.

As discussed above, FLASHForward is a new beamline, currently in the commissioning phase. Design started in 2013, first components were installed in 2016, and majority of the beamline installation was completed in Summer 2017. Shortly after, first beams were sent to the new beamline. Conceptually FLASHForward consists of the following sections (see Figure 3):

- *Extraction.* Here the beams are extracted from FLASH2 using two fast pulsed dipoles, thus not affecting normal FLASH2 user operation<sup>1</sup> and transported to the FLASH2 tunnel, separated from the main FLASH tunnel by a safety wall.
- *Compression.* Allows additional longitudinal post-compression of the beams, thanks to the variable longitudinal compression ( $R_{56}$ ).
- *Final focusing.* Starts after the final bending dipole which makes the beamline parallel to FLASH2. Allows transverse shaping of the beams before the interaction with the plasma.
- *Plasma chamber.* Here interaction with the plasma takes place.
- *Diagnostics section.* Allows measurement of properties of the beams, outgoing from the plasma. Includes the **electron spectrometer**, a device used to measure energy spectrum of electrons, and central topic of this work.

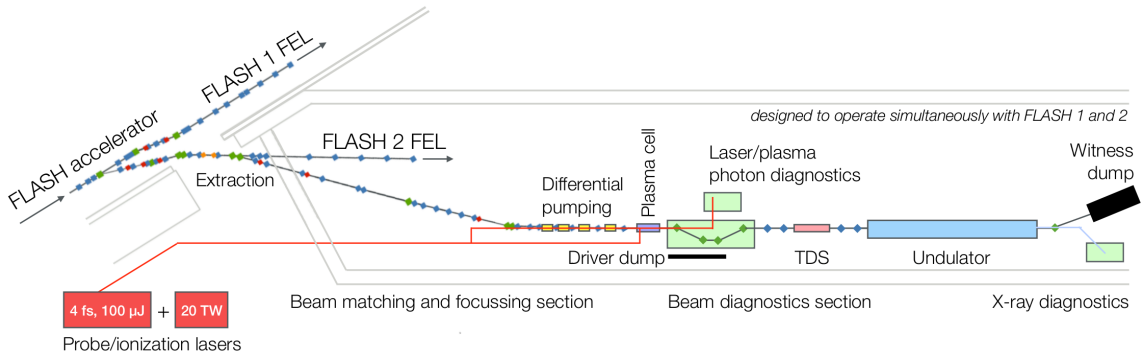


Figure 3: Layout of FLASHForward.

<sup>1</sup>In 2017, static dipole magnets were used, which prevents simultaneous operation of FLASH2 and FLASHForward.



- *FEL beamline.* Contains undulators to produce FEL radiation using plasma-accelerated beams.

This report focuses on one of the principal elements in the diagnostics section, the electron spectrometer, in particular on the analysis of the magnetic field distributions and on determination of the energy resolution, a crucial parameter of the spectrometer.

### 3 Electron Spectrometer for FLASHForward

Electron energy measurement is essential for plasma-wakefield acceleration experiments. When the drive beam excites the wakefield, it loses energy, due to the decelerating fields in the front of the ion cavity. The longer the propagation distance in the plasma, and the stronger the field in the cavity, the more energy will be lost to the wakefield. Therefore, detection of a significant fraction of electrons with energies below the original driver energy indicates that the wakefield is driven and allows quantification of the energy transfer efficiency. On the other hand, the witness beam gains energy; detection of electrons with energies higher than the original driver beam energy clearly indicates that acceleration by the wakefield took place.

The principle of the FLASHForward electron spectrometer is illustrated in the Figure 4. A vacuum chamber is placed in a magnetic field. Electrons entering the chamber are deflected by the field; low-energy electrons are deflected stronger than high-energy electrons, resulting in a spatial distribution, where position corresponds to energy. In other words the energy distribution of electrons is translated to their spatial distribution. Therefore, by measuring the spatial distribution, the energy distribution can be determined. At FLASHForward, the spatial distribution is measured by scintillating phosphor screens read out by CCD cameras.

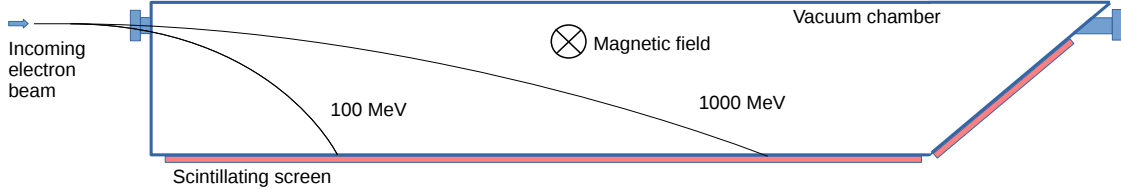


Figure 4: Principle of electron spectrometer at FLASHForward. See text for more details.

A crucial property of the spectrometer is its *energy resolution*, since it defines the smallest feature in the energy spectrum which can be resolved. For the case of energy measurement at FLASHForward, the resolution must be significantly smaller than the relative difference between the initial drive beam energy and the witness energy, in order to demonstrate the acceleration of the witness beam.

In this work, resolution is evaluated with help of particle tracking simulations using the measured three-dimensional distribution of the magnetic field. In addition, the measured magnetic field maps are studied in detail, which is important not only for the analysis of the resolution of the broadband spectrometer, discussed in this work, but also for other applications of this magnet at FLASHForward (later, it is planned to use another magnet of this type as a high-resolution, narrow-band spectrometer together with a transverse-deflecting structure).

## 4 Magnetic field analysis

### 4.1 DORIS III dipole magnet

The magnetic field which disperses the electrons (as discussed in Section 3) is provided by a dipole magnet recycled from the DORIS III 4.5 GeV electron storage ring. This is a sector magnet, meaning that nominally the beam enters (exits) the magnet perpendicularly to its entrance (exit) face. The nominal bending angle is  $5^\circ$ . The cross-section of the magnet is shown in Figure 5 and its main properties are summarised in the Table 1.

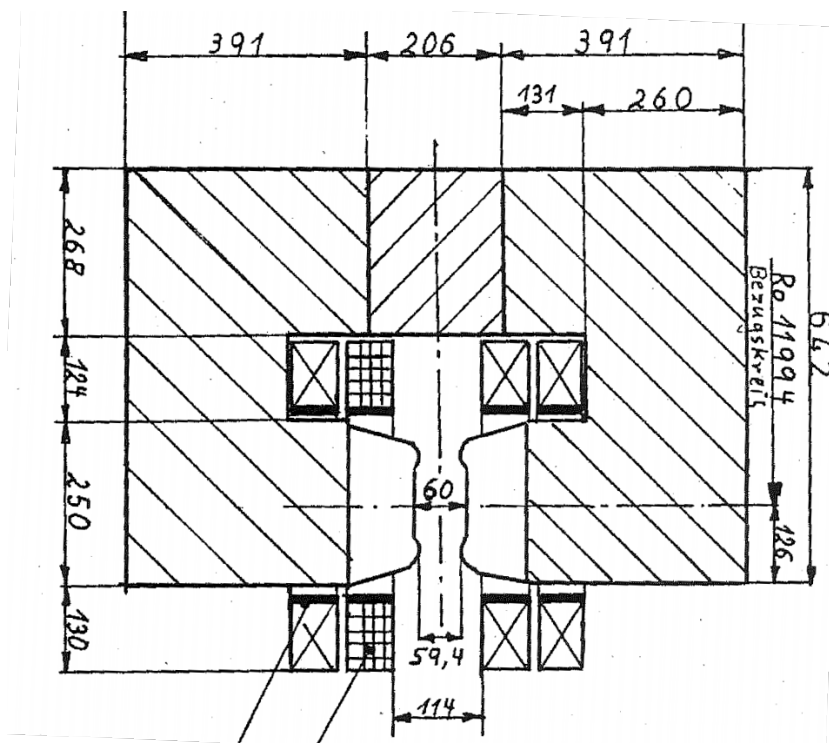


Figure 5: Cross-section of the DORIS III dipole magnet. Electron beam enters the magnet perpendicularly to the drawing plane. Taken from [4].

Magnet type	C-shape, sector
Bending angle	$5^\circ$
Maximum Magnetic Field	1.4 T
Maximum current	950 A
Pole Length	1020 mm
Pole width	60 mm
Gap width	200 mm

Table 1: Properties of the DORIS III dipole magnet [4].

### 4.2 Magnetic Field Measurements

Detailed knowledge of the three-dimensional distribution of the magnetic field inside the magnet is crucial for reliable evaluation of the resolution. Prior to the summer student

program, the MEA group of DESY performed such measurements. In this section, these data are analysed.

The coordinate system for the measurement is shown in Figure 6. It is a right-handed Cartesian system with the origin in the center of the magnet. The  $x$ -axis is pointing vertically,  $y$ -axis is horizontal (perpendicular to the poles), and  $z$ -axis is pointing along the nominal beam propagation. Symmetry of the magnet was employed to reduce the amount of measurements: only half of the magnet for 1D and 2D measurements, and a quarter for 3D measurements was measured. A three-dimensional Hall sonde was used for the measurements, meaning all three components of the field are available. In addition, *hysteresis curves* (see section 4.4) were measured with a rotating coil, which provides the longitudinal magnetic field integral.

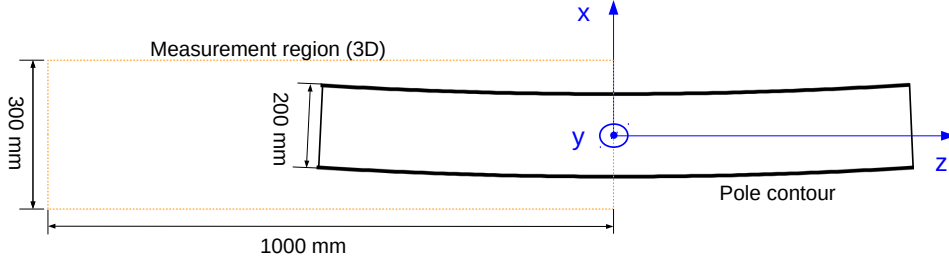


Figure 6: Definition of the coordinate system for the magnetic measurements. The beam enters the magnet from the left. The  $5^\circ$ -curvature is visible. The area where the three-dimensional map was measured, is shown.

### 4.3 One-dimensional field map

The one-dimensional map was measured along the nominal orbit (also called *design orbit*), defined as a straight line outside the magnet gap, and  $5^\circ$  circular arc inside it, as illustrated in the Figure 7. As discussed in section 4.2, only half of the magnet is measured, therefore  $z < 0$ .

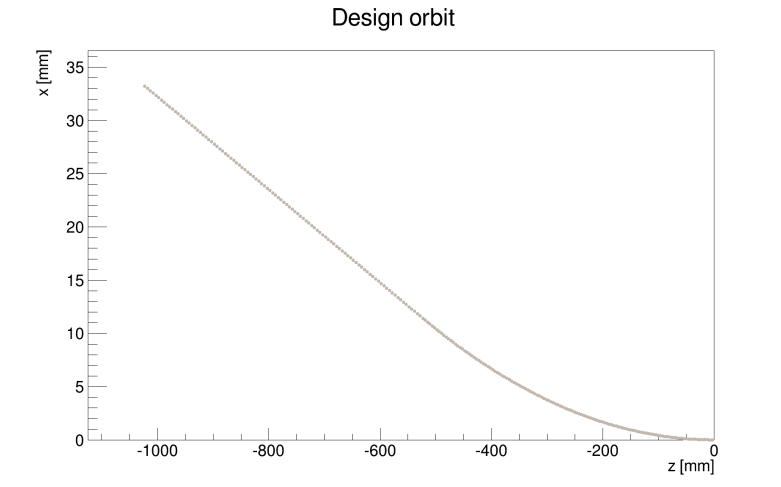


Figure 7: Trajectory used for 1D measurements.



The dominant component in a dipole magnet is the transverse component,  $B_y$ . It is shown as a function of the longitudinal coordinate (path along the orbit) defined as  $s_n = \sum_{i=1}^n \sqrt{\Delta x_i^2 + \Delta z_i^2}$  for different currents in Figure 8. This definition holds strictly outside the magnet, and the error due to a circular orbit inside the magnet is small due smallness of the grid step. As expected for a dipole magnet, the field is practically

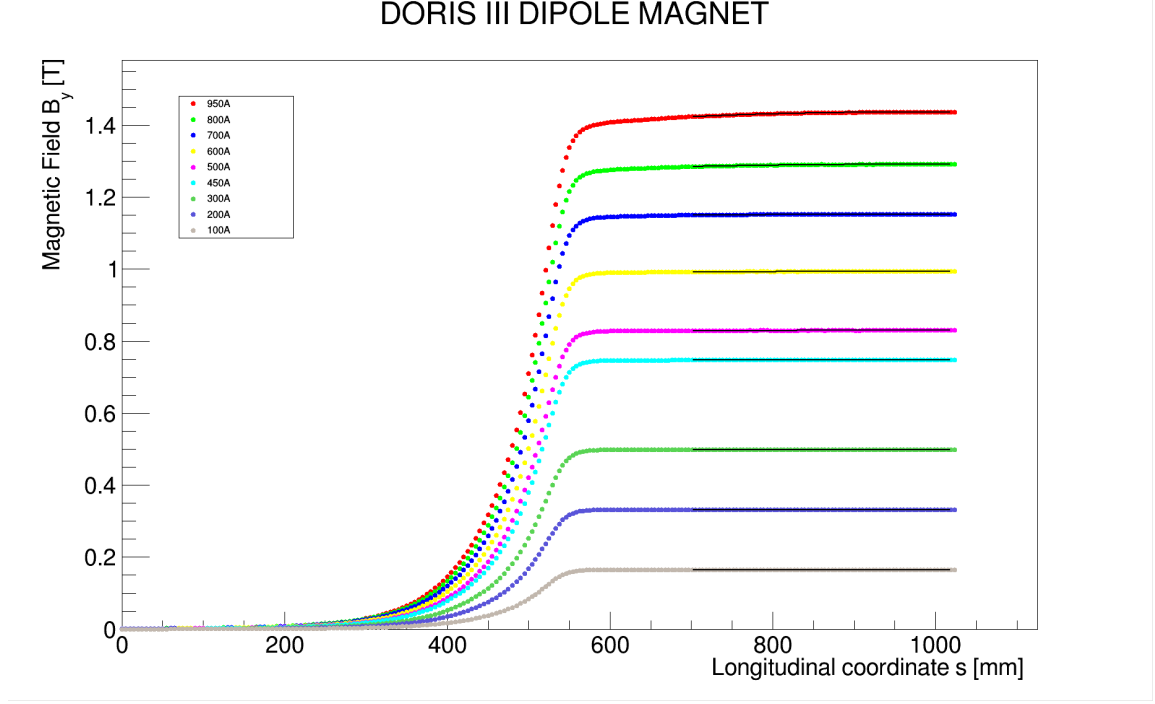


Figure 8:  $B_y$ -component as a function of the longitudinal coordinate  $s$ .

constant inside the magnet ( $s > 500$  mm). However, for higher currents, a non-linear dependence is observed, which can be attributed to *saturation effects*. It can be also seen that large fields exist outside the magnet ( $s < 500$  mm), so-called *fringe fields*. In order to quantify the effect from the fringe fields, the *effective magnetic length* is commonly introduced. It is defined as:

$$L_{eff} = \frac{\int_{-\infty}^{\infty} B_y ds}{B_y^{\max}},$$

where  $B_y^{\max}$  is the maximum field for a given current, and the integral is taken along the design orbit.  $B_y^{\max}$  was evaluated by fitting the dependencies shown in Figure 8 with a second-order polynomial. The integral was evaluated numerically from the measured data, taking into account that only half of the magnet was measured, that is up to  $z = 0$  mm. The resulting effective length as a function of current is shown in Figure 9. It can be noted that it stays practically constant with current, which is an indication that the field distribution does not change dramatically with current.

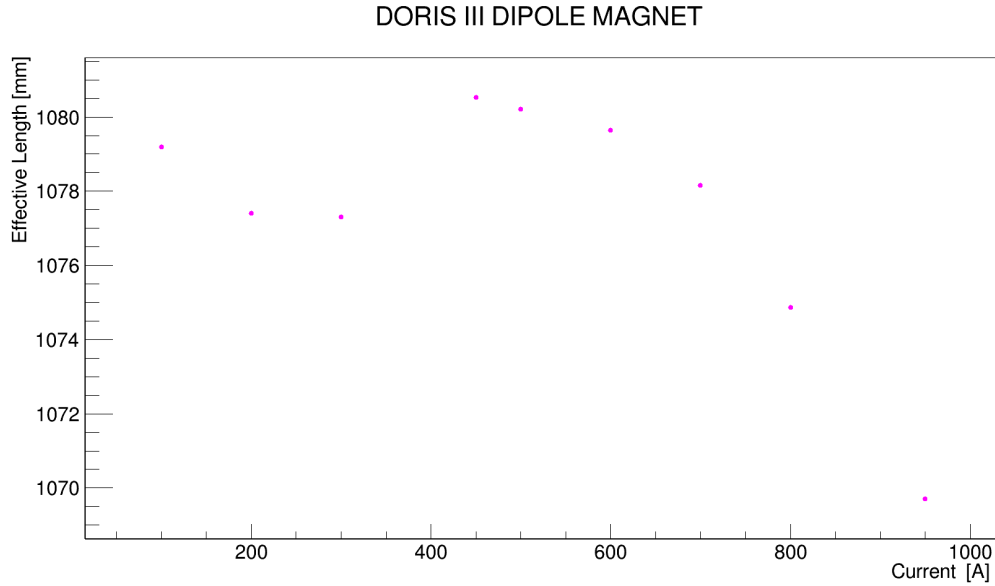


Figure 9: Effective length as a function of current. See text for more details.

#### 4.4 Hysteresis Curve

*Hysteresis curve* is a dependence of the magnetic field on current,  $B(I)$ . The most important feature here is that there is no unique functional dependence, namely the field  $B$  depends not only on current  $I$ , but also on the previous magnetisation history. For example, in general case magnet will show non-zero magnetic field even in the absence of current,  $B(0) \neq 0$ . However after a demagnetisation procedure (cyclic change of the current with decreasing amplitude, ending ultimately at  $I=0$ ), there will be no field if the current is not applied. In practice, hysteresis curve measurements are performed with the so-called rotating coils which directly measure the integral of the field along the coil. Note, that in the previous section, the magnetic field integral was evaluated by integrating a one-dimensional profile obtained with a Hall probe. For the measurements described in this work, a 2-meter long rotating coil was used, which is sufficient to take into account the fringe fields (see Figure 8). Three  $B(I)$  dependencies were measured:

- *The new curve* is obtained for positive currents, namely from 0 A to maximum magnet current of 950 A. The first step is a demagnetisation procedure which ensures that  $B = 0$  for  $I = 0$ . Afterwards, the current is increased by 50 A and the magnetic field integral is measured for each current.
- *The lower hysteresis branch* is obtained for both positive and negative currents, namely from -950 A to 950 A. Prior to the measurement, the current is set to -950 A. It is then ramped to 950 A, and then back to -950 A. This cycle is repeated 10 times. Afterwards, the current is incremented with 50A steps from -950A to 950A (10 A steps in the range [-100, 100] A), and the magnetic field is measured at each step.
- *The upper hysteresis branch* is measured by decreasing current from 950 A to -950A, directly after the measurement described in the previous item, using the same current steps.

All three curves for the DORIS III magnet are depicted in the Figure 10. On this scale they appear as a single curve. One can see that for small currents, the dependence is practically linear, while for higher currents a non-linear behaviour appears, which is due to saturation. Integrals calculated from 1D-profiles are also shown. They are consistent with the rotating coil measurements, as expected. The plot also shows a dependence with the linear term subtracted. The linear term was determined from a fit to the new curve in the region  $I \in [0, 300]A$ . After the subtraction one can clearly distinguish the three curves.

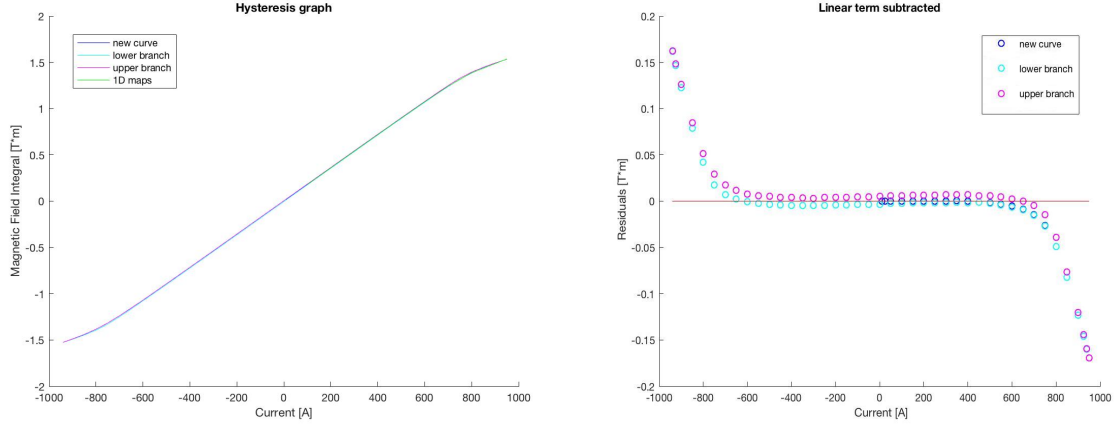


Figure 10: Hysteresis curve before (left) and after (right) linear term subtraction.

## 4.5 Three-dimensional field maps

The three-dimensional (3D) field map, that is a dependence of the magnetic field on all three spatial coordinates, is especially important for simulations described in this work. The reason for this is that spectrometer is designed as *broadband*, in other words it has a large energy acceptance. Namely, electron beams entering the magnet have a large energy spread and therefore do not move close to the design orbit, but rather spread over a large region of the magnet (see Figure 4). Hence, knowledge of the field in the large area of the magnet is important. Figure 6 shows the measurement region in the  $xz$ -plane. Figure 11 shows the  $B_y$  component of the field of the 3D map on the plane  $y = 0$ . Dependencies on  $z$  for  $x = 0$  and on  $x$  for  $z = 0$  on this plane are also shown. The  $z$ -dependence clearly resembles the 1D profile, consistent with expectations. Figures 19 and 20 in the appendix show the  $B_x$  and  $B_z$  components, respectively. These components can have potentially harmful effects on spectrometer operation (for example, the  $B_x$ -component introduces horizontal force, which deteriorates horizontal divergence measurement). However, the magnitudes of these components, as the figures show, are at least three orders of magnitude smaller than the main  $B_y$ -component.

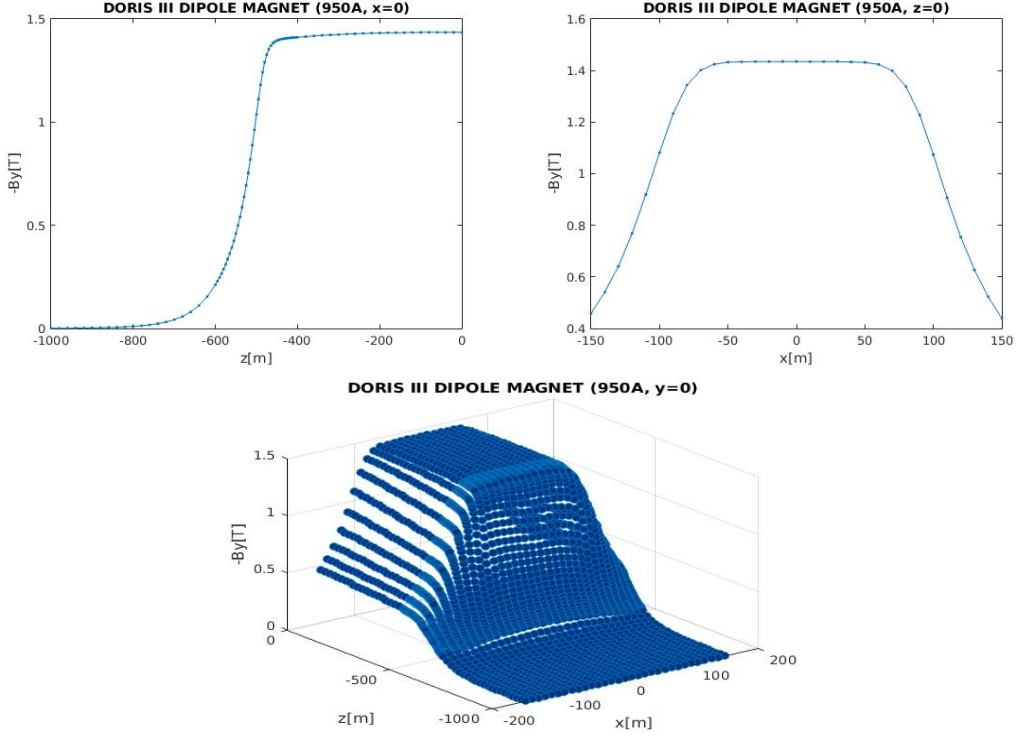


Figure 11:  $B_y$  component on the plane  $y = 0$ . See text for more details.

## 5 Tracking simulations and resolution determination

Three-dimensional tracking simulations were performed in order to determine the range of electron energies that spectrometer can detect, to establish the *energy calibration curve*, that is the dependence of coordinate on energy, and to evaluate the spectrometer resolution. The CST simulation package was used. The 3D CAD model (see Figure 18) and the 3D field map, analysed in the previous chapter, were used for the simulation, in order to provide a realistic modelling of the system. CST allows definition of arbitrary particle sources. Six-dimensional phase-space distribution of the beam has to be specified, namely the initial position (three coordinates) and the initial momentum (three components) for each particle must be given.

In order to evaluate the energy calibration curve, a beam with no divergence (that is all particles initially move along the  $z$  axis) and a large energy spread was defined. The distance from the source to the magnet center was set to 3 m. Electron trajectories from this simulation are shown in Figure 12. For each particle, an intersection point with the scintillating screens (see Figure 4) was determined. Figure 13 shows the relation between the electron energy and the  $z$ -coordinate of this intersection, that is the energy calibration curve. A fifth-order polynomial fit to this dependence is also shown.

The final quantity that has to be estimated is the *resolution*. The dominant effect defining the resolution is the vertical beam divergence. Namely, if electron has initially a non-zero vertical momentum component ( $p_x \neq 0$ ) it will have a different  $z$ -coordinate on the scintillating screen, compared to an electron moving on-axis ( $p_x = 0$ ). Therefore there is a certain ambiguity in energy determination, which depends on the beam divergence. In general, the resolution is defined as the full-width at half-maximum (FWHM) of the *detector response function*. In order to calculate it, the beam divergence is set to some

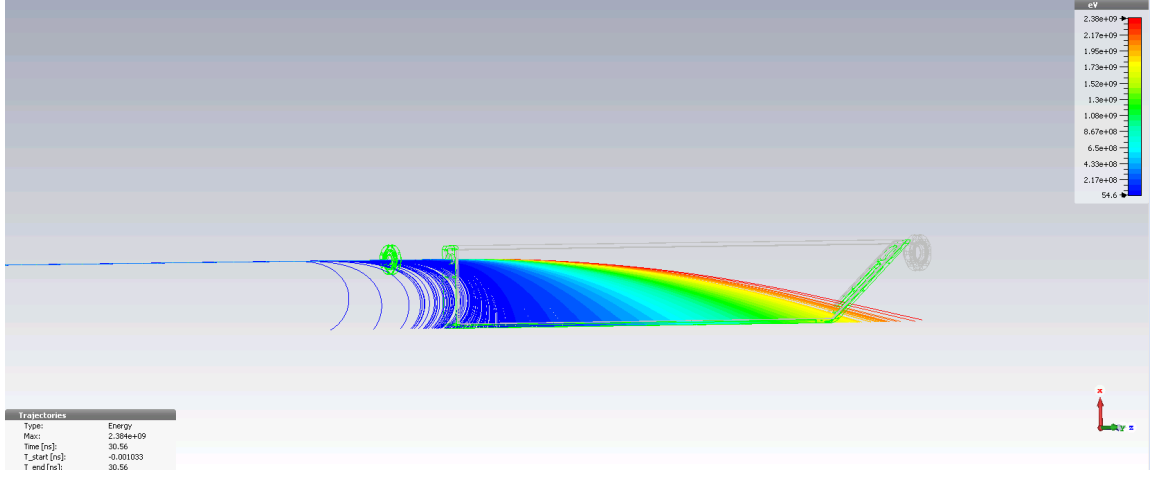


Figure 12: Trajectories inside the spectrometer chamber.

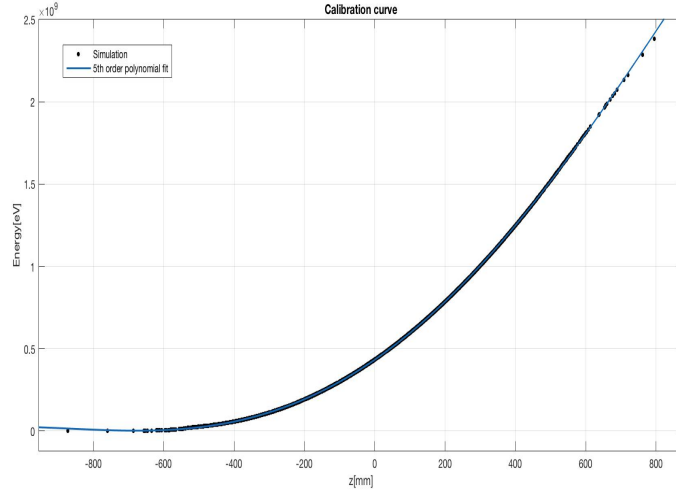


Figure 13: Energy calibration curve.

predefined value, while the energy spread is set to zero. The relative resolution  $\sigma_r$  is defined as

$$\sigma_r(E) = 2.355 \frac{\sigma(E)}{E},$$

where  $E$  is the beam energy and  $\sigma$  is the standard deviation of the detector response function, determined from a gaussian fit. The coefficient 2.355 is used to convert the standard deviation to FWHM. Figure 14 shows the obtained resolution as a function of energy for an r.m.s. divergence of 1 mrad.

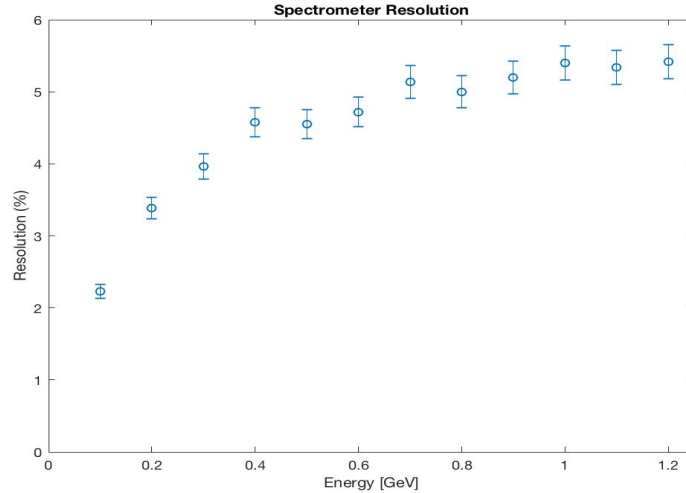


Figure 14: Spectrometer resolution.

## 6 Conclusions

In this work, the electron spectrometer for FLASHForward plasma-wakefield acceleration experiment was studied. The magnetic field maps of the DORIS III dipole magnet, chosen for the spectrometer, were analysed. The effective length has been determined and compared for different currents. No significant dependence on current was found. Hysteresis curves were analysed and compared to the integrals calculated directly from the 1D-profiles. Three-dimensional tracking simulations were performed. The energy calibration curve was determined. Resolution due to the beam divergence (assuming 1 mrad r.m.s.) was determined and was found to be in the range from 2% to 5%, sufficient to detect driver energy loss and witness energy gain.

As a summary, this work confirms the suitability of the spectrometer for the planned plasma-wakefield experiments at FLASHForward and provides valuable information for its operation.

## References

- [1] T. Tajima and J. M. Dawson, *Laser Electron Accelerator*, Phys. Rev. Lett. **43**, 267-270 (1979)
- [2] P. Chen et al. *Acceleration of electrons by the interaction of a bunched electron beam with a plasma*, Phys. Rev. Lett. **54**, 693-696 (1985)
- [3] A. Aschikhin et al., *FLASHForward Facility at DESY*, Nucl. Instr. Meth. **A 806**, 175-183 (2016)
- [4] Y. Holler, H. Wuempelmann, *Modifizierung der Magnete fuer DORIS III*, DESY-Report M-91-03 (in German)
- [5] Y. Holler, *private communication*.



## A Additional figures



Figure 15: Layout of FLASH1, FLASH2 and FLASHForward.

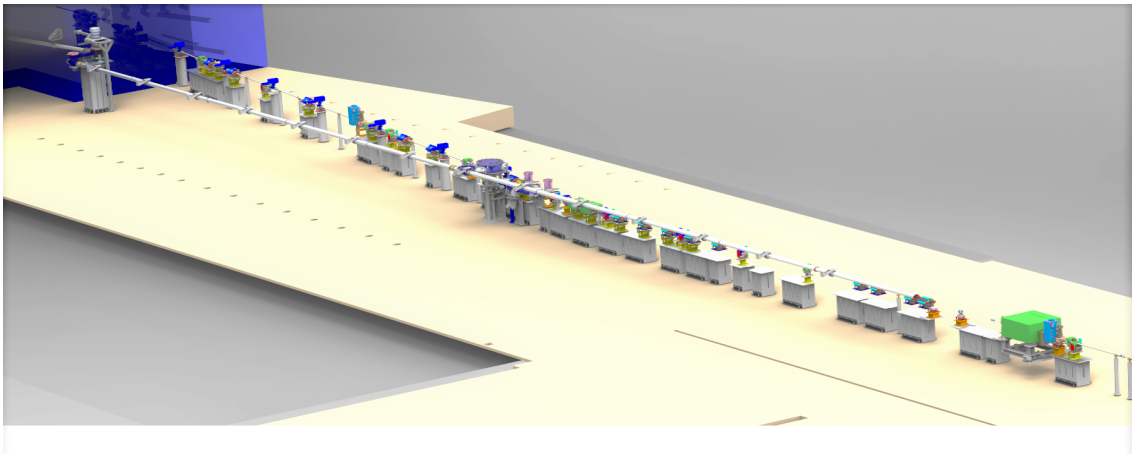


Figure 16: FLASHForward CAD Model.

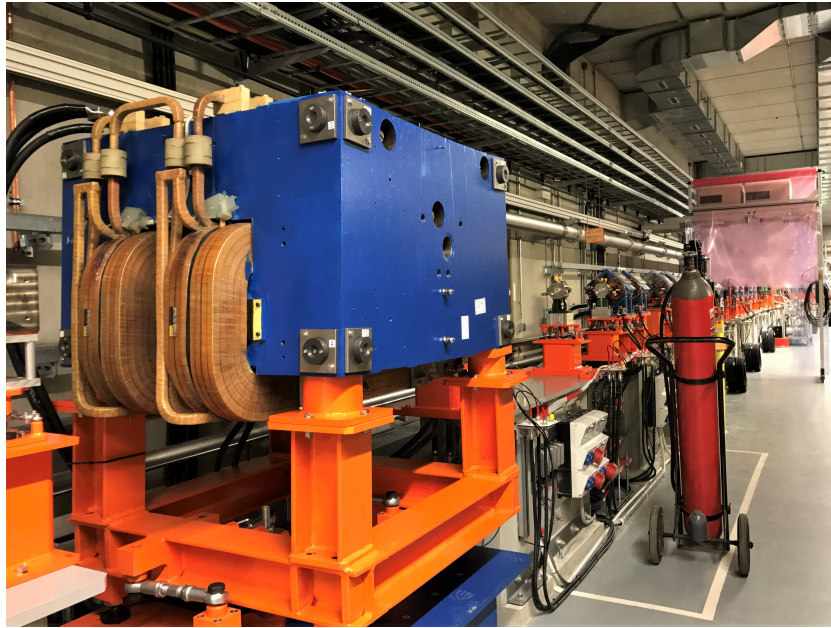


Figure 17: Spectrometer magnet inside the tunnel.

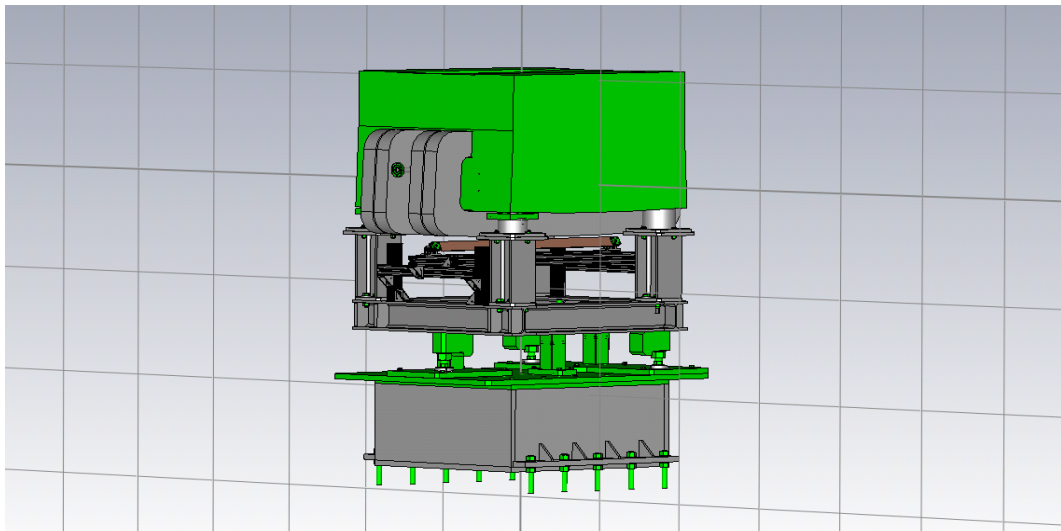


Figure 18: 3D CAD Model of the spectrometer.

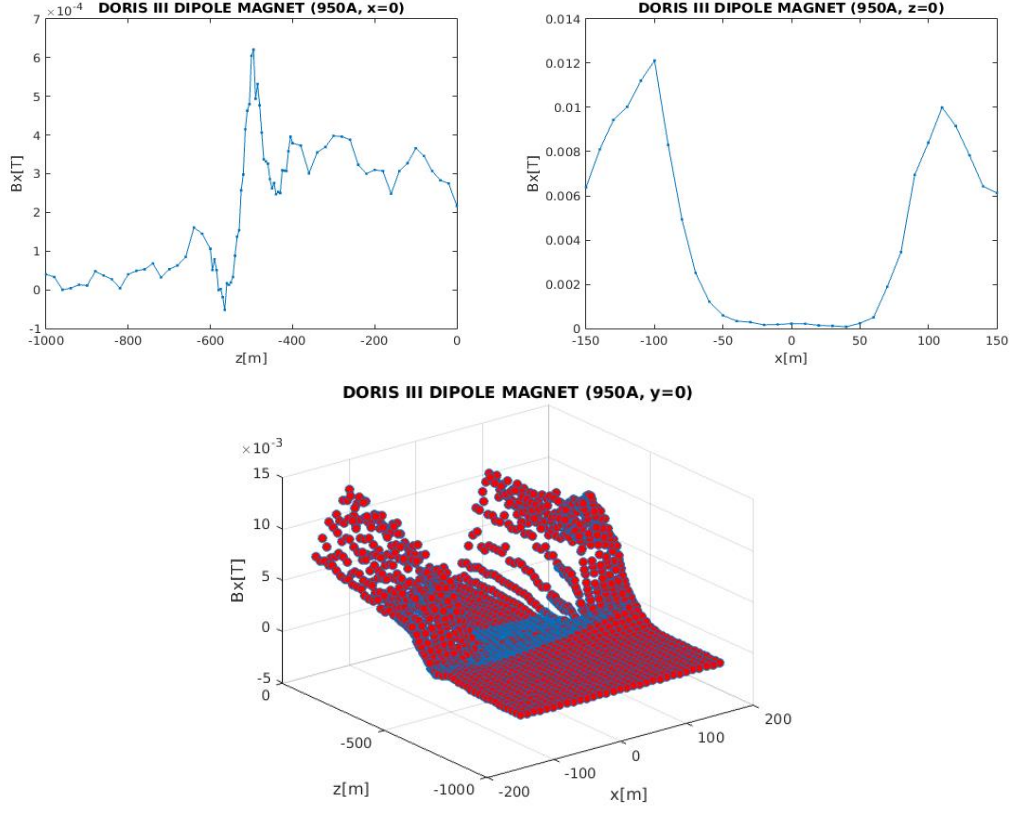


Figure 19:  $B_x$  component on the plane  $y = 0$ . See text for more details.

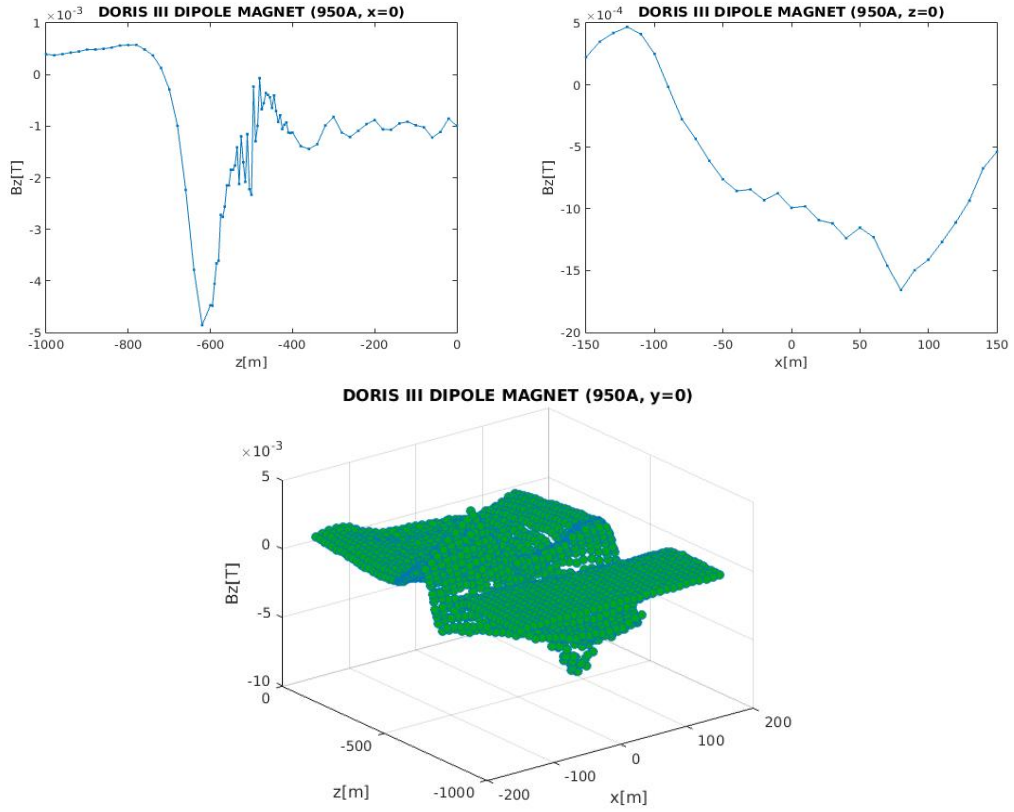


Figure 20:  $B_z$  component on the plane  $y = 0$ . See text for more details.